Progress In Electromagnetics Research C, Vol. 59, 89–99, 2015

Dielectric Resonator Antenna Arrays for Microwave Energy Harvesting and Far-Field Wireless Power Transfer

Ahmed Z. Ashoor and Omar M. Ramahi*

Abstract—This paper presents dielectric resonator antennas (DRAs) for efficient energy harvesting or wireless power transfer in the microwaves regime. A single DRA and 1×3 array were used to build foundation profiles for DRAs as energy absorbers. The proposed structures were designed and fabricated to resonate around 5.5 GHz. The study examined different factors that affect the absorbed power efficiency. The size of ground plane and coupling between dielectric resonator (DR) elements in an array were studied, highlighting their effects on the overall efficiency of the antenna structure for different incident polarizations. A 5×5 array was built based on the studied factors and tested numerically and experimentally. Measurements showed that energy absorption efficiency as high as 67% can be achieved using an array of DR antennas.

1. INTRODUCTION

Several researchers have studied energy absorption from electromagnetic waves to provide power to broad range of low-power devices using primarily metallic antennas such as microstrip patches, spiral antennas and metamaterial cells [1–9]. Apart from severe metallic losses or low radiation efficiencies when operating in high frequencies, it was found that metallic antennas generally offer narrow impedance bandwidths [10]. On the other hand, Dielectric Resonator Antennas (DRAs), which are considered as non-metallic antennas [11], offer some advantages when compared to metallic antennas [5]. Particularly, DRAs provide high radiation efficiency, wide bandwidth and compact size in the microwave frequency range [10–12].

The resonant frequency of DRA is a function of size, shape and dielectric permittivity [13]. The impedance bandwidth for DRAs is a function of the dielectric permittivity and aspect ratio (length-to-height) [12]. Thus, for a given dielectric permittivity (ε_r), the aspect ratio can be adjusted to provide compact low profile antenna or a wide-bandwidth. The dimensional degrees of freedom are considered when comparing different geometries of the DRAs (in fact, a proper choice may depend upon the desired bandwidth, directivity or volume [11, 13]). The DRA can tolerate relatively high temperatures (in comparison to metallic antennas), thus, its resonant frequency remains stable with temperature fluctuation [14]. This advantage makes DRAs highly suitable for applications in harsh environments such as military applications [14] and remotely powered sensors in uncontrolled environments [15].

DRAs can be designed in smaller size than conventional metallic antennas ($1/\sqrt{\varepsilon_r}$). Using high permittivity constant for compact designs, DRAs offer wider bandwidth compared to microstrip antennas [5, 13].

Good energy absorption call for minimal Ohmic and dielectric losses such that the power absorbed is maximized [1]. The work in [5] showed that DRAs have negligible losses and thus offer higher radiation efficiency in the microwave regime when compared to microstrip patch antennas. DRAs offer

Received 15 July 2015, Accepted 8 September 2015, Scheduled 10 September 2015

* Corresponding author: Omar M. Ramahi (oramahi@uwaterloo.ca).

The authors are with the School of Electrical and Computer Engineering, University of Waterloo, Waterloo, Ontario N2L 3G1, Canada.

compatibility with existing feeding techniques which make them easy to fabricate using current circuit and microwave printed technology [11, 16]. The design in [17] of a rectangular DRA fed by a metallic waveguide showed the ability of low-temperature co-fired ceramic technology to integrate dielectric and metal layers in a single process. Such techniques can be employed to design DRAs and to integrate them in highly compact packages.

This paper focuses on using DRAs for energy absorption in the microwave regime. The emphases will be on the ability of DRA, as a single antenna or in array arrangement, to efficiently absorb microwave energy and convert the energy of the field into a usable AC power. The AC power can be converted into DC using classical rectification circuitry. We emphasize that the conversion from AC to DC is *not* the subject of this work as it can be found in many excellent research and application papers (good examples can be found in [18–21]). In particular, this paper highlights the importance of mutual coupling between adjacent elements on the absorbed power efficiency. Experiments are presented to validate the numerical simulation [22].

2. PROOF OF CONCEPT

DRAs can be designed in a variety of shapes. Basic DR shapes are generally used due to their ease of analysis and simple fabrication [4]. In this work, a rectangular DR was chosen as it offers advantages over the hemispherical and cylindrical geometries [11, 23]. Hemispherical and cylindrical DRAs offer no degree and one degree of freedom, respectively. On the other hand, rectangular DRs have two degrees of freedom, also referred to as the aspect ratios (hight/length and width/length). Because of these two aspect ratios, designers have flexibility in selecting the proper ratio to suit the needs of the intended application. These degrees of freedom offer design choices when controlling the antenna bandwidth, operating frequency, and excitation mechanisms [11, 13]. In this work, the DRA specifications were determined such that the antenna resonates at 5.5 GHz. This frequency was chosen partially based on the material availability.

The following approach was taken to design single rectangular DRA. Initially, two material constraints were imposed, the DR hight ($b = 6.35\,\text{mm}$) and dielectric constant ($\varepsilon_r = 9.8$). Then the DR dimensions (see Fig. 1) were calculated by employing the Dielectric Waveguide Model (DWM) formula for a rectangular dielectric resonator [23]. The DWM was used to solve for the desired resonant frequency as follows:

$$k_x \tan(k_x a/2) = \sqrt{(\varepsilon_r - 1)k_{mn}^2 - k_x} \tag{1}$$

where:

$$\begin{aligned} &k_{mn} = 2\pi f_{mn}/v \\ &k_y = \frac{m\pi}{c} \quad k_z = \frac{n\pi}{2b} \\ &k_x^2 + k_y^2 + k_z^2 = \varepsilon_r k_{mn}^2 \end{aligned} \tag{2}$$

In Eqs. (1) and (2), m and n are positive integers corresponding to the field variation in the y and z directions, respectively, and f_{mn} is the resonant frequency of the (m, n) mode. v is the speed of light in free space, and ε_r is the dielectric constant of the resonator. a, b, and c are the dimensions of the dielectric resonator (DR).

The DWM set of equations can be used to determine the dimensional parameters of the resonator for a desired frequency of operation when constraining some of the parameters. Based on the solutions of Eqs. (1) and (2), different possible rectangular DR dimensions can be obtained that satisfy the desired resonant frequency. Thus, by using the above DWM set of equations solving for the lowest TE modes and constraining the height to $b = 6.35\,\text{mm}$ and permittivity to $\varepsilon_r = 9.8$, a single DRA was designed to operate at 5.5 GHz and then simulated using ANSYS HFSS [24]. After minor optimization to achieve resonance at 5.5 GHz, the dimensions of the DR were found to be $a = 16.5\,\text{mm}$ and $c = 11.4\,\text{mm}$. The DR was centered on a ground plane with $W' = L' = \lambda/2$ as shown in Fig. 1. We note that the values for W' and L' were the result of optimization such that the ground plane was minimized while maximizing the DRA return loss and radiation efficiency. This setup gave a ground plane size of width $W = 38\,\text{mm}$ and length $L = 33\,\text{mm}$. An HRM(V)-306S SMA type $50\,\Omega$ probe feeder was used with outer radius of 2.05 mm and inner conductor radius of 0.64 mm (these values were taken from the specifications sheet).

The inner conductor of the probe that connects to the body of the DR has a length of $h = 5.37\,\text{mm}$ and was positioned at $c/2$ on y-axis and at $s = 2.4\,\text{mm}$ on x-axis as shown in Fig. 1. The resulting simulated Return Loss (RL) and simulated input impedance of the DRA are shown in Figs. 2(a) and 2(b).

Following [7], the energy absorption efficiency was defined based on the footprint area of the structure. This definition measure how efficient the absorber is in converting the available incident microwave power, P_{in}, to an average AC power, P_{out}. The available power P_{in} is dependent on the footprint (real estate) occupied by the absorber. Thus, the overall efficiency of the absorber η_{eff} was defined as the ratio of the total time average power P_{out} to the available microwave power P_{in} available at the absorber footprint area and dependent only on the incident plane wave, its propagation direction and polarization. The efficiency is given by:

$$\eta_{eff} = P_{out}/P_{in} \tag{3}$$

A plane wave was used as the source of incident field. An impedance sheet that matched the DRA input impedance of $50\,\Omega$ was placed at the feeding port. This sheet was used to calculate the AC power that would be made available by the DRA.

Since the efficiency of the absorber was defined based on its physical footprint, including any ground plane, it is expected that the size of the ground plane will change the absorption efficiency levels. The ground plane size was defined by placing the DR at the middle of a ground plane and varying W' and L' proportionally to the DRA free-space wavelength of $\lambda = 54.5\,\text{mm}$ in the particular case considered (see Fig. 1). Variations in W' and L' were taken from 0 to $\lambda/2$. For instance, having $W' = L' = \lambda/2$ gave a ground plane size of $W = 71.1\,\text{mm}$ and $L = 66\,\text{mm}$, where a $W' = L' = 0$ gave a ground size of ($W = 16.5\,\text{mm}$ and $L = 11.4\,\text{mm}$).

To calculate the absorption efficiency of the single DRA, the structure was simulated with normal incidence ($\theta = 0$ and $\Psi = 0$) plane waves for different ground plane sizes. The resulting power efficiency

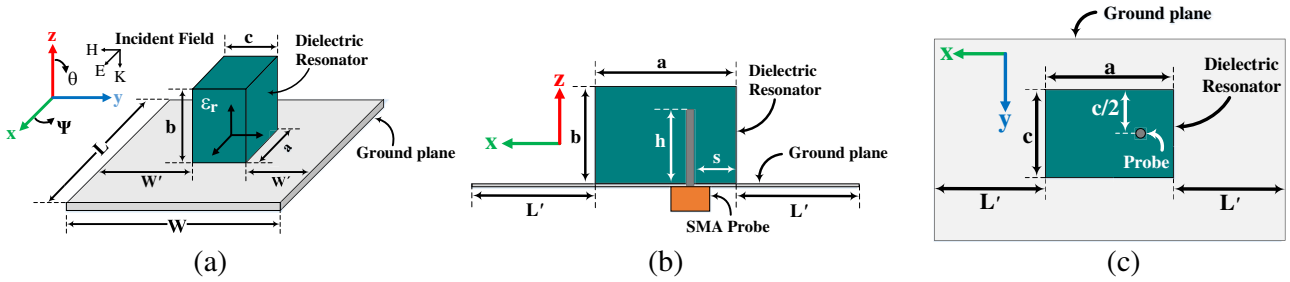

Figure 1. Schematic showing a single DRA placed on a conducting ground plane fed by an SMA probe: (a) Perspective view, (b) side view and (c) top view showing the probe location.

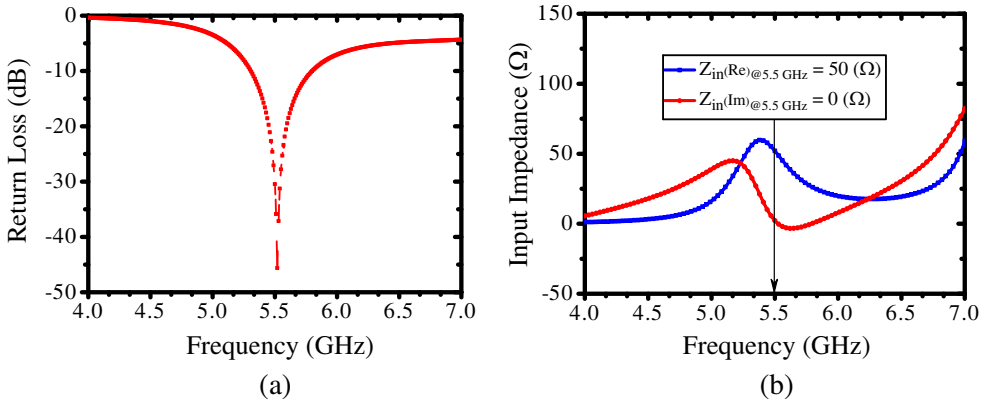

Figure 2. (a) Simulated return loss (S_{11}) of the single rectangular DRA. (b) Simulated input impedance of the single rectangular DRA: real and imaginary parts.

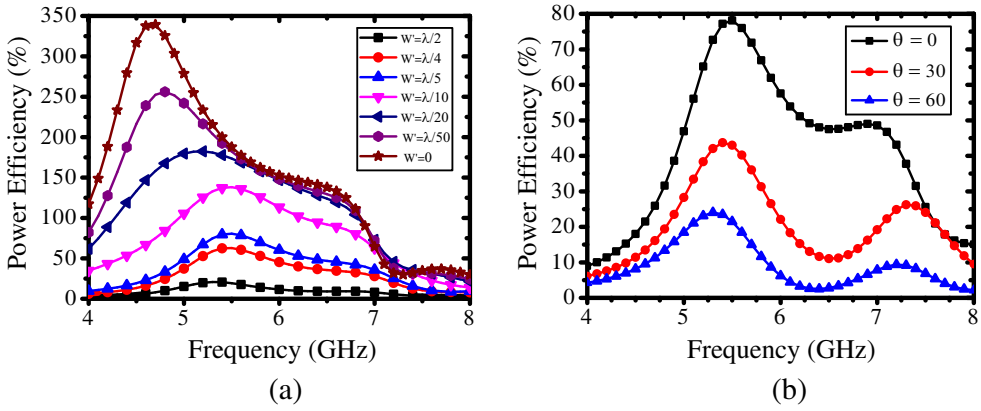

Figure 3. (a) The effect of the single DRA ground plane size on the simulated power efficiency with a normally incident illumination $\theta = 0$ and $\Psi = 0$ ($W' = L'$; see Fig. 1). (b) Simulated power efficiency of a single DRA with ground size spacing of $\lambda/5$ for three different incident illuminations $\theta = 0$, $\theta = 30$, and $\theta = 60$ where $\Psi = 0$.

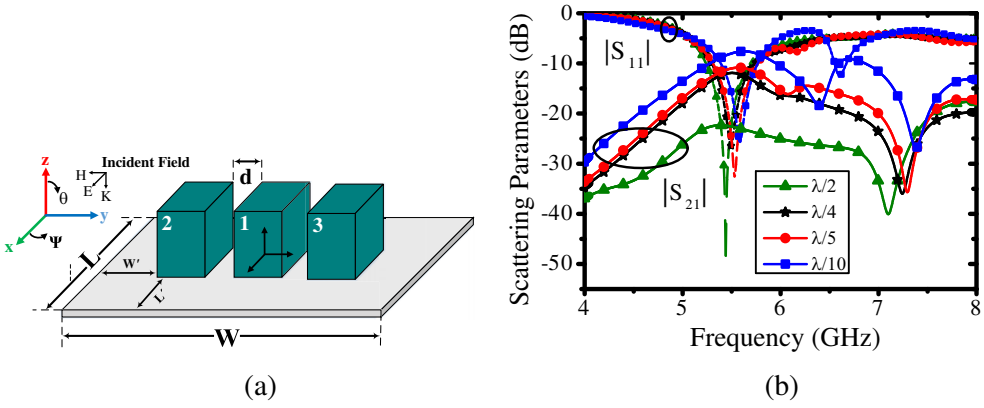

Figure 4. (a) Schematic showing a DRA array of 1×3 unites placed on a conducting ground plane with an inter-element spacing d between each against element. (b) Simulated 1×3 DRA array scattering parameters S_{11} and S_{21} for different inter-element spacings d.

for various ground plane sizes are shown in Fig. 3(a). In Fig. 3(b), we fixed the ground plane size at $W' = L' = \lambda/5$ (corresponding to $W = 38.3\,\text{mm}$ and $L = 33.5\,\text{mm}$) and show the efficiency for three different incident angles $\theta = 0$, $\theta = 30$, and $\theta = 60$ where $\Psi = 0$. We observe that the smaller the ground plane, the higher the efficiency. This conclusion, although not intuitive, does not necessarily imply that the smaller the ground plane, the higher the power absorbed by the DRA. It need to be kept in mind that the efficiency definition is based on the total footprint of the entire antenna structure.

Next, we consider a one-dimensional 1×3 DRA array shown in Fig 4(a). A arrays are typically used to improve the antenna gain and directivity [25]. Spacing between array elements introduces mutual coupling that affects the radiation property of each array element. In most antenna communication applications where gain enhancement is the goal, an inter-element spacing of $\lambda/2$ between array elements is generally used to provide, not full, but sufficient isolation between adjacent antennas [26]. The 1×3 DRA array was designed using the dimensions used above for the single rectangular DRA. In particular, we focused on the effect of mutual coupling and size of ground plane on the efficiency.

The power absorbtion efficiency of the array elements were studied for different ground plane sizes and for different inter-element spacing d while setting $W' = L' = d$ (see Fig. 4(a)). Each element was fed by a $50\,\Omega$ coaxial probe. First, the scattering parameters of the array middle element (S_{11}, S_{12}, and S_{13}) were simulated to show the impact of mutual coupling. Fig. 4(b) shows the scattering parameters

for different inter-element spacings. Because of symmetry, only S_{11} and S_{12} are shown in Fig. 4(b). Amongst the cases considered, the $\lambda/2$ inter-element spacing gave the least mutual coupling.

The array was illuminated by a plane wave for different incident angles $\theta = 0$, $\theta = 30$, and $\theta = 60$ where $\Psi = 0$ (refer to Fig. 4(a) for illumination angles). Lumped impedances of 50 Ω were placed at all ports to simulate the received power from each array element. The total available power received by the three elements is given by

$$P_{out} = \sum_{n=1}^{N} p_{out}^{(n)} \tag{4}$$

where N is the number of elements in the array and $p_{out}^{(n)}$ the received power from each array element.

Two investigations were considered to study factors that may affect the absorption efficiency for the array. First, a fixed ground plane size of $W = 2.6\lambda$ and $L = 1.3\lambda$ was used while the inter-element spacing d was varied proportionally to the free-space wavelength $\lambda = 54.5$ mm from 0 to $\lambda/2$. The simulation results are shown in Fig. 5(a). Here, our interest lies mainly in the effect of the elements coupling on the efficiency.

The second investigation was to study the effects of varying both the inter-element spacing d

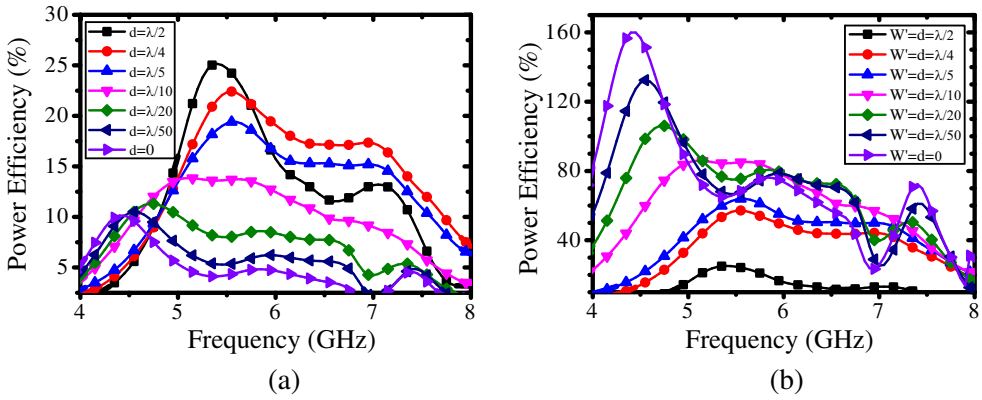

Figure 5. (a) Normal incidence ($\theta = 0$ and $\Psi = 0$) simulated power efficiency of the 1×3 array illuminated by a plane wave for a fixed ground plane size of $W \times L = 2.6\lambda \times 1.3\lambda$ and different inter-element spacings $d = \lambda/2$, $\lambda/4$, $\lambda/5$ and $\lambda/10$ (see Fig. 4(a)). (b) Simulated power efficiency of the 1×3 array illuminated by a plane wave for different ground plane sizes and inter-element spacings between elements $W' = d = \lambda/2$, $\lambda/4$, $\lambda/5$, $\lambda/10$, $\lambda/20$, $\lambda/50$, and 0 ($W' = L'$; see Fig. 4(a)).

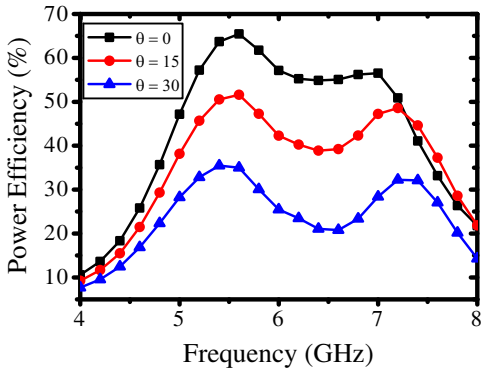

Figure 6. Simulated power efficiency of a 1×3 array illuminated by a plane wave for three different incident illuminations $\theta = 0$, $\theta = 15$, and $\theta = 30$ where $\Psi = 0$ for ground plane size and inter-element spacing of $\lambda/5$.

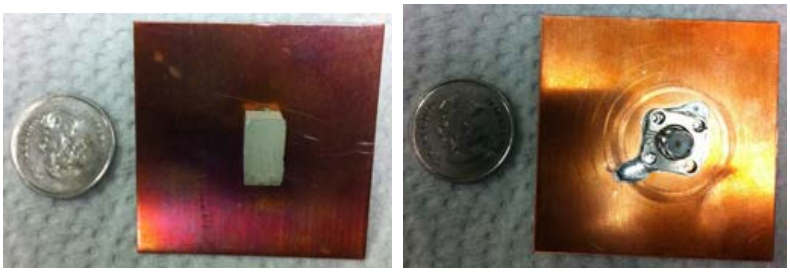

(a) (b)

Figure 7. Fabricated single DRA fed by a SMA coaxial probe: (a) Top view and (b) bottom view.

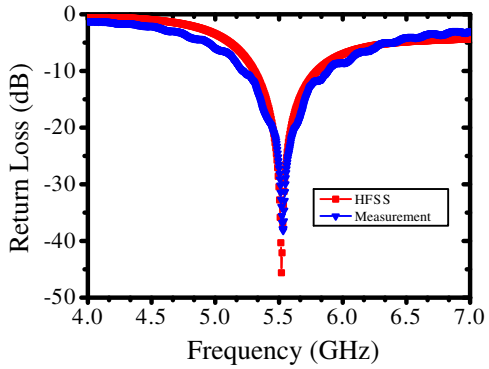

Figure 8. Simulation and measurement return loss (S_{11}) of the single rectangular DRA.

between array element and the ground plane size on efficiency. The variation of the ground plane size was defined similarly to the above study for the single DRA ground by centering the middle element and varying $W' = L'$ proportionally to the DRA free-space wavelength $\lambda = 54.5\,\text{mm}$ (refer to Fig. 4(a)). Variations of the ground plane sizes and the inter-element spacing d between element were taken simultaneously from 0 to $\lambda/2$. For instance, $W' = L' = d = \lambda/4$ gave a ground plane size of $W = 88.8\,\text{mm}$ and $L = 43.8\,\text{mm}$. The simulated power efficiency of the 1×3 DRA array having different ground plane sizes and inter-element spacings between elements is shown in Fig. 5(b). We note that both Fig. 5(a) and Fig. 5(b) have identical plots for the case of $\lambda/2$ inter-element spacing, when the maximum power efficiency reaches approximately 25%.

Different incident angles on the array were then simulated for the case of $W' = L' = d = \lambda/5$. Fig. 6 compares the 1×3 DRA array power efficiency for three different incident angles $\theta = 0$, $\theta = 15$, and $\theta = 30$ where $\Psi = 0$.

3. 5×5 DRA ARRAY

The purpose of the above study was to obtain preliminary results as to what factors have an effect on the DRA absorption efficiency when used as a single element or in array configuration. Next, we consider the case of a two dimensional 5×5 array where the study will be based on numerical simulation as well as experiments.

We consider a DRA array of 5×5 elements. The above study of the single DRA element and 1×3 array built foundation bases to determine positions of the coaxial probe and inter-element spacings. The following design specifications were taken to simulate and build the 5×5 DRA array. Probes were positioned at $a/2$ on y-axis and at $s = 2.4\,\text{mm}$ x-axis (refer to Fig. 1 for probe position). DR dimensions were of $a = 16.5\,\text{mm}$, $b = 6.35\,\text{mm}$, and $c = 11.4\,\text{mm}$. Rogers TMM10i material was used as DRs. The inter-element spacing between adjacent elements d and the ground plane size $W' = L'$ were chosen to be of $\lambda/5$. This made an array of a ground plane size of $W = 122.6\,\text{mm}$, $L = 148\,\text{mm}$ and inter-element

spacing d of 10.9 mm (refer to Fig. 1 and Fig. 4(a) for probe position and array geometry). Holes of 0.64 mm radius (SMA inner conductor) were drilled in all DRs. Each DR was terminated with an SMA having 50 Ω input impedance. The top and bottom face of the fabricated 5×5 DRA array is shown in Fig. 9.

A single DRA was fabricated using the dimensions and specifications mentioned in the previous section. This was done before performing any simulation or fabrication of the 5×5 array. The fabricated single DRA is shown in Fig. 7. Rogers TMM10i having dielectric constant $\varepsilon_r = 9.8$ was used as the DR material. The DR was mounted on copper ground plane of 1 mm thick. A 50 Ω SMA coaxial probe was used to feed the antenna. The return loss of the fabricated DRA is shown in Fig. 8 and compared to the simulation result.

In a large array, the characteristics of all elements will be identical except those elements at or close to the boundary of the array. Therefore, to gauge the general performance of the fabricated array working frequency, the reflection coefficient S_{11} of the center element was measured (shown circled in Fig. 9) while all other array elements were terminated with 50 Ω loads. The measured S_{11} was extracted using an Agilent 8722ES Vector Network Analyzer (VNA) while the simulation was performed using ANSYS-HFSS. Fig. 10 shows good agreement between the two results.

Next, we study the performance of the 5×5 array as a microwaves energy absorber. The study is carried out numerically and experimentally. Fig. 11(a) shows the simulation setup using ANSYS HFSS where the DRA array was illuminated by a horn antenna placed at a distance of 100 cm. The array was illuminated by plane waves with different incident angles. The simulated power efficiencies are shown in Fig. 12(a) for three different incident angles.

Figure 11(b) shows the measurement setup for testing the 5×5 array. A broadband horn antenna (0.7 GHz to 18 GHz frequency range with a maximum gain of 14.71 dB) was used as the source of

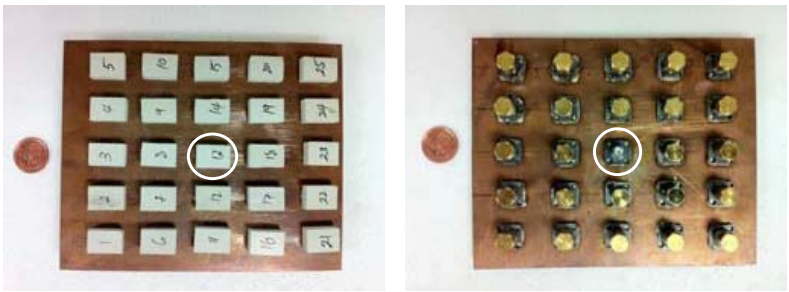

(a) (b)

Figure 9. Fabricated 5×5 DRA array where all ports are terminated by 50 Ω except the centered element (circled) to measure its return loss: (a) Top view and (b) bottom view.

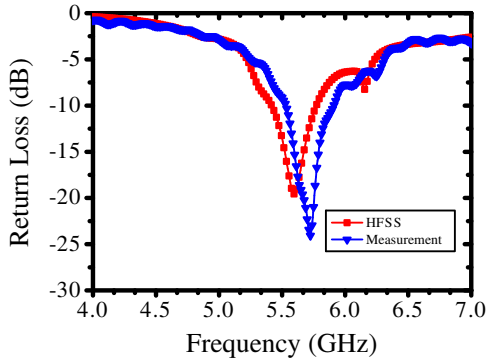

Figure 10. Simulation and measurement of the return loss for the central element of the 5×5 DRA array.

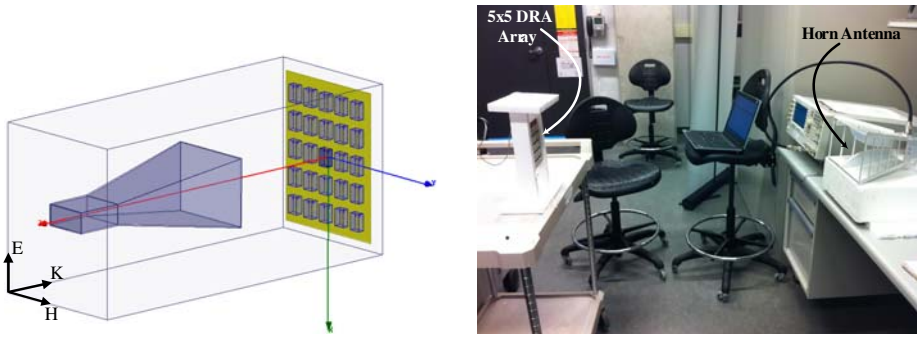

(a) (b)

Figure 11. (a) Simulation setup of the 5×5 DRA array illuminated by a horn antenna. (Note: Distance between the horn and array is not to scale). (b) Measurement setup of the 5×5 array in the absorption mode which shows the horn antenna (right side) as a source and the DRA array under test (left side) where the distance in between is 100 cm.

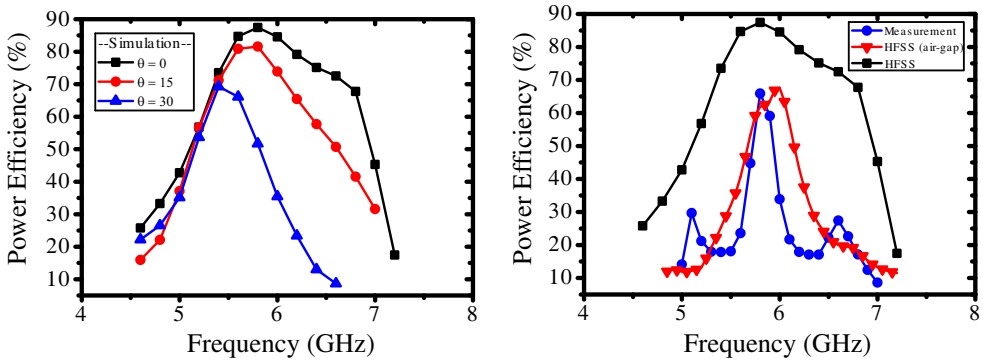

(a) (b)

Figure 12. (a) Power efficiency of the 5×5 array for three different incidents $\theta = 0$, $\theta = 15$, and $\theta = 30$ where $\Psi = 0$. (b) Power absorbing efficiency of the 5×5 array.

electromagnetic power. The horn was powered by an Agilent E8257D Signal Generator. The array was placed at a distance of 100 cm from the horn antenna.

Each array element contributes differently to the measured receiving power over the testing frequency range of 5 GHz to 8 GHz. Since we are testing for the maximum power that can be absorbed by the entire array, the power received by each element $p_{out}^{(n)}$ was measured while terminating all other ports with 50 Ω load as shown in Fig. 9. An Agilent E4448A PSA Spectrum Analyzer was used to measure the received power. The impact of cable losses connected between the array and the spectrum analyzer was considered when calculating the total absorbed power of the array P_{out}. The total absorbed power P_{out} received by the array were then calculated using Eq. (4).

The power provided by the horn antenna at the array plane P_{in} was calculated using the following equations:

$$P_{in} = P_t \times \textbf{array area} \tag{5}$$

where:

$$P_t = \frac{P}{4\pi R^2} G_t(f) \tag{6}$$

P_t is the radiated power density generated by the horn at the location of the structure (receiving antenna) but without the structure present, P the power fed to the transmitting antenna's (horn) input terminal, and $G_t(f)$ the gain of horn antenna as a function of frequency. In the above equation, only the area of the array was used to measure the effective aperture of the array. Normally, however,

Friis equation [25] uses the gain of the array over a spherical area to measure the effective aperture of antennas. In addition, impact of gain level over the testing frequency was considered in calculating the power provided by the horn antenna. The impact of the cable losses connected between the horn and the signal generator was also measured over the testing frequency of 5 GHz to 8 GHz. These considerations have ensured accurate measurements of the power P_t provided by the horn antenna. The available power at the array, P_{in}, was then calculated, from which the overall power efficiency of the array was obtained using Eq. (5).

The maximum measured efficiency obtained for the 5×5 array was found to be 67% as shown in Fig. 12(b). This obtained efficiency was different from the simulated one which gave a maximum efficiency of 88% with wider bandwidth coverages as shown in Figs. 12(a) and 12(b). Careful scrutiny of the fabricated array revealed gaps between the DR and the conductor surface of the probe. These gaps can cause an impedance mismatch between the DR and its feeder [27] which, in turn, affects the power absorption efficiency. To include this effect, air gaps were introduced in the simulated DRA array between the DRs and their feeding probes. The gaps were simulated by adding annular vacuum layer of thickness 0.5 mm surrounding the feeding probes. This makes the hole's radius of the DRs 1.14 mm instead of 0.64 mm (which is also the feeding probe's radius). Good agreement is observed between the measurements and simulation when air gaps were included in the simulation as clearly shown in Fig. 12(b).

4. DISCUSSION

The study of the single rectangular DRA has proved the capability of the antenna as energy absorber. The numerical simulation results showed that the power efficiency for a single DRA could reach a maximum of 80%. Maintaining high efficiency levels over wide bandwidth depends on the antenna probe position. The simulation of the single DRA also showed that the ground plane size has a significant impact on the absorption efficiency. The smaller the ground plane, the higher the absorption efficiencies. However, this conclusion applies to a single DRA and does not necessarily imply that the smaller the ground plane, the higher the absorbed power. For a single antenna in general, the absorbed energy is not limited to the precise footprint of the antenna, which in the case of the DRA, comprises the ground plane. This is because the near field of the antenna, which depends on the wavelength, extends beyond the ground plane. Therefore, the single DRA analysis is only intended to achieve preliminary conclusion about parameters that can affect the absorption efficiency.

For the 1×3 DRA array, inter-element spacing d between array elements was found to be an important factor that influences the array efficiency. For instance, an efficiency of 20% was obtained for the 1×3 array of $\lambda/5$ inter-element spacing with a fixed ground plane (refer to Fig. 5(a)). The efficiency with the same inter-element spacing was dramatically increased to 80% when the ground plane sized of $W' = L' = \lambda/5$ (refer to Fig. 5(b)). In addition, when the array elements were placed with almost zero separation with a ground plane covering the area of the elements, an absorption efficiency of 160% was obtained. The range of frequency that gives higher level of efficiencies was shifted from the resonance frequency of 5 GHz by 1 GHz.

For the 5×5 DRA array, the design specifications were chosen based on the studied single DRA and 1×3 array. The array was simulated and fabricated using $W' = L' = d = \lambda/5$. Air gaps were noticed when performing the measurement for the fabricated 5×5 array. This factor was considered as another important factor besides the probes position that influences the level of power absorbtion efficiency. These gaps were due to imprecise drilling in the DRs that resulted in wider holes than the dimensions of the feeding probes. As a result, impedance mismatching occurred between the DR elements and their feedings. This mismatching directly affects the overall absorption efficiency. In the simulation and prior to introducing air gaps between the feeding probe and the DR, high efficiency levels between 69% and 88% were achieved over wide range of frequencies and for different incident angles. Introducing air gaps lowered the efficiency levels and narrowed the frequency band. Good agreement was obtained between measurements and simulations that accounted for air gaps. Clearly, more precise fabrications lead to higher energy efficiency levels.

Finally, we note that recently published works showed that ensembles of metamaterial particles provide higher absorption efficiency than the DRA array presented here. In fact, in [28], a near-unity

absorption was achieved. Comparison between the structure presented here and those reported in the literature cannot be easy as there are variety of factors that need to be considered including the frequency bandwidth and the range of incident angles over which a specific level of energy absorption takes place. For meaningful comparison, structures need also to be tested for their energy absorption effectiveness for different incident field polarizations. Additionally, fabrication material and cost differ sharply between dielectric resonator structures and metallic patches. All these factors make quantitative and systematic comparison difficult.

5. CONCLUSION

This paper presents DRAs as a new candidate for microwave energy absorption. A single and an array DRA have been studied and designed. The study has combined both simulation and measurement. The analyses included the effects of different ground plane sizes, array inter-element spacing, and positions of feeding probes. Comparisons between power efficiencies of the different configurations and different field incident angles were presented. In particular, a 5×5 DRA array was fabricated and tested showing measured power absorbing efficiency close to 70%.

ACKNOWLEDGMENT

The authors like to acknowledge the Saudi Arabian Ministry of Higher Education and the support of the Natural Sciences and Engineering Research Council, Canada. We also acknowledge CMC Microsystems for the provision of products and services that facilitated this research, including CAD tools and test support.

REFERENCES

1. Harb, A., "Energy harvesting: State-of-the-art," *Renewable Energy*, Vol. 36, No. 10, 2641–2654, Oct. 2011.
2. Paradiso, J. and T. Starner, "Energy scavenging for mobile and wireless electronics," *IEEE Pervasive Computing*, Vol. 4, No. 1, 18–27, Jan. 2005.
3. Ukkonen, L., L. Sydanheimo, and M. Kivikoski, "Effects of metallic plate size on the performance of microstrip patch-type tag antennas for passive RFID," *IEEE Antennas and Wireless Propagation Letters*, Vol. 4, 410–413, Dec. 2005.
4. Jan, J.-Y. and L.-C. Tseng, "Small planar monopole antenna with a shorted parasitic inverted-l wire for wireless communications in the 2.4-, 5.2-, and 5.8-GHz bands," *IEEE Transactions on Antennas and Propagation*, Vol. 52, No. 7, 1903–1905, Jul. 2004.
5. Lai, Q., G. Almpanis, C. Fumeaux, H. Benedickter, and R. Vahldieck, "Comparison of the radiation efficiency for the dielectric resonator antenna and the microstrip antenna at Ka band," *IEEE Transactions on Antennas and Propagation*, Vol. 56, No. 11, 3589–3592, Nov. 2008.
6. Jabbar, H., Y. Song, and T. Jeong, "RF energy harvesting system and circuits for charging of mobile devices," *IEEE Transactions on Consumer Electronics*, Vol. 56, No. 1, 247–253, Feb. 2010.
7. Ramahi, O. M., T. S. Almoneef, M. Alshareef, and M. S. Boybay, "Metamaterial particles for electromagnetic energy harvesting," *Applied Physics Letters*, Vol. 101, No. 17, 173 903–173 903-5, Oct. 2012.
8. Alavikia, B., T. S. Almoneef, and O. M. Ramahi, "Electromagnetic energy harvesting using complementary split-ring resonators," *Applied Physics Letters*, Vol. 104, No. 16, 163 903–163 903-4, Oct. 2014.
9. AlShareef, M. and O. M. Ramahi, "Electrically small particles combining even- and odd-mode currents for microwave energy harvesting," *Applied Physics Letters*, Vol. 104, 253 906–253 906-4, 2014.
10. Leung, K.-W., E. H. Lim, and X. S. Fang, "Dielectric resonator antennas: From the basic to the aesthetic," *Proceedings of the IEEE*, Vol. 100, No. 7, 2181–2193, Jul. 2012.

11. Luk, K. M. K. and K. W. K. Leung, *Dielectric Resonator Antennas*, Research Studies Press, Philadelphia, Baldock, England; Institute of Physics Publishing, Philadelphia, 2003.
12. Petosa, A., A. Ittipiboon, Y. Antar, D. Roscoe, and M. Cuhaci, "Recent advances in dielectric-resonator antenna technology," *IEEE Antennas and Propagation Magazine*, Vol. 40, No. 3, 35–48, Jun. 1998.
13. Petosa, A., *Dielectric Resonator Antenna Handbook*, Artech House, London, 2007.
14. Chen, Y.-C., S.-M. Tsao, C.-S. Lin, S.-C. Wang, and Y.-H. Chien, "Microwave dielectric properties of 0.95mgtio(3)-0.05catio(3) for application in dielectric resonator antenna," *Journal of Alloys and Compounds*, Vol. 471, No. 1–2, 347–351, Mar. 2009.
15. Akyildiz, I., W. Su, Y. Sankarasubramaniam, and E. Cayirci, "A survey on sensor networks," *IEEE Communications Magazine*, Vol. 40, No. 8, 102–114, Aug. 2002.
16. Kingsley, J. W., R. Thomas, and S. Williams, "Attaching antenna structures to electrical feed structures," US Patent 7,183,975, Feb. 2007.
17. Roy, L., N. Berthereau, N. Hojjat, K. Kautio, and H. Panesaar, "Dielectric resonator antenna with microstrip-waveguide transition in LTCC," *Electronics Letters*, Vol. 42, No. 19, 1078–1079, Sep. 2006.
18. Zbitou, J., M. Latrach, and S. Toutain, "Hybrid rectenna and monolithic integrated zero-bias microwave rectifier," *IEEE Transactions on Microwave Theory and Techniques*, Vol. 54, No. 1, 147–152, Jan. 2006.
19. Hagerty, J., F. Helmbrecht, W. McCalpin, R. Zane, and Z. Popovic, "Recycling ambient microwave energy with broad-band rectenna arrays," *IEEE Transactions on Microwave Theory and Techniques*, Vol. 52, No. 3, 1014–1024, Mar. 2004.
20. McSpadden, J., L. Fan, and K. Chang, "Design and experiments of a high-conversion-efficiency 5.8-ghz rectenna," *IEEE Transactions on Microwave Theory and Techniques*, Vol. 46, No. 12, 2053–2060, Dec. 1998.
21. Harouni, Z., L. Cirio, L. Osman, A. Gharsallah, and O. Picon, "A dual circularly polarized 2.45-GHz rectenna for wireless power transmission," *IEEE Antennas and Wireless Propagation Letters*, Vol. 10, 306–309, Apr. 2011.
22. Ramahi, O. M. and A. Ashoor, "Dielectric resonator antennas and arrays for electromagnetic energy harvesting," US Provisional Patent Application No. 62035265, Aug. 8, 2014.
23. Kumar Mongia, R. and A. Ittipiboon, "Theoretical and experimental investigations on rectangular dielectric resonator antennas," *IEEE Transactions on Antennas and Propagation*, Vol. 45, No. 9, 1348–1356, Sep. 1997.
24. ANSYS HFSS Version 15.0.0, Ansys Inc., http://www.ansys.com.
25. Balanis, C. A., *Antenna Theory: Analysis and Design*, 3rd Edition, John Wiley, Hoboken, NJ, 2005.
26. Petosa, A., R. Mongia, A. Ittipiboon, and J. Wright, "Design of microstrip-fed series array of dielectric resonator antennas," *Electronics Letters*, Vol. 31, No. 16, 1306–1307, Aug. 1995.
27. Junker, G., A. Kishk, A. Glisson, and D. Kajfez, "Effect of an air gap around the coaxial probe exciting a cylindrical dielectric resonator antenna," *Electronics Letters*, Vol. 30, No. 3, 177–178, Feb. 1994.
28. Almoneef, T. S. and O. M. Ramahi, "Metamaterial electromagnetic energy harvester with near unity efficiency," *Applied Physics Letters*, Vol. 106, No. 15, 153902, 2015.